ELECTRIMACS 2019 – Salerno, Italy, 21st-23rd May 2019

High granularity model of a photovoltaic array under complex shadow conditions

Luis GARCIA-GUTIERREZ · Michael BRESSAN · Antonino SFERLAZZA · Fernando JIMENEZ · Salvador DE-LAS-HERAS · Corinne ALONSO

Abstract This paper presents a model of Photovoltaic (PV) array under complex partially shading conditions integrating characteristics of shadow area and combination of direct and indirect radiations. The area of the shadow on PV module is deducted through of image processing. The Hybrid Bond-Graph (HBG) facilitates the energy exchange between the different parts of the PV module justifying the high granularity of the tool. The proposed model is validated through experimental tests under shading conditions

1 Introduction

In the last few years, solar or PV systems has received much attention for the ease of implementation. However, the use of this source through PV array generators is affected by limits caused by the low efficiency-per-m^2 of conversion devices, the shadows and the not efficient working conditions due to electrical mismatch [1]. Two kinds of shadows can be visible on PV module: the homogeneous shadows which induce a drop of PV production and the non-homogeneous shadows such as trees, soiling drastically affect the electrical generation of PV array [2]. The shading of a PV cell or of a group of cells can lead to a phenomenon denoted as hot-spot [3]. This can produce a permanent damage of the shaded cell, with a consequent reduction of the provided power despite the activation of the by-pass diodes [4]. Several authors developed modeling approaches to treat the complexities arising from non-uniform environmental conditions in PV systems operation [5]. Others models were developed to understand the impact of the shadows on the PV module performances [6–8]. PV model used a system of equations and linear interpolation which usually employ simple and easy-to-use expressions. Gutierrez Galeano [9] presented the study of a simplified approach which models and analyzes the performance of partially shaded PV modules using shading ratio. This approach integrates the characteristics of shaded area and shadow opacity into the model. However, this method needs simultaneous I-V curves measurements and recording to construct the model. It is important to develop models with great details that allow to analyze and better understand the electrical behavior of PV systems. The core of this paper is the development of model allowing to represent the I-V curves of a PV module under complex shading conditions. The high level of granularity of the model permits to represent accurately the I-V curves thanks to irradiation, cell temperature and shadow parameters. The method consists in analyzing the area of shadow and the direct and indirect radiation that receives each PV cell. Thanks to an image processing, it is easier to give an area of shadows which affects the PV module. Hybrid Bond-Graph (HBG) is used to analyze the variation of energy on each cell under complex shading conditions. This paper is organized as follows: Section 2 shows the proposed model of PV module including the shadow parameters. Section 3 presents the image processing to give the area of the shadow on PV module. Section 4 treats about the results of the comparison between the I-V curves of the model with experimental I-V curves to validate the proposed model. Section 5 shows the conclusion of the work.

Luis GARCIA-GUTIERREZ
Universidad de los Andes, Cra 1 N 18A - 12, 111711,
Bogotá, Colombia, e-mail: la.garcia11@uniandes.edu.co

Corinne ALONSO
Université Toulouse III - Paul Sabatier-LAAS-CNRS
7, avenue du Colonel Roche BP 54200, 31031 Toulouse cedex 4,
France,e-mail: alonsoc@laas.fr

2 Proposed PV model for complex shading conditions

2.1 General Shaded PV-cell model

The photovoltaic effect is the conversion of light into electricity. Most of the models in the literature do not take into account the effect of the reverse bias [10]. A precise model was proposed by Bishop [11] which incorporates the avalanche effect as a non-linear multiplier factor that affects the shunt resistance current term as shown below:

$$I = I_{ph} - I_o\left[e^{\frac{V_c+IR_s}{V_t}} - 1\right] - \frac{V_c+IR_s}{R_{sh}}\left[1+k\left(1-\frac{V_c+IRs}{V_{br}}\right)^{-n}\right] \quad (1)$$

where I_{ph} is the generated photo-current (A), I_o is the reverse saturation current (A), R_s is the series resistance (Ω), R_{sh} is the shunt resistances (Ω), V_{br} is the breakdown voltage (V), k and n are constants. The photo-current I_{ph} is the electric current through a cell in function of the irradiation that receives the PV cell, and its temperature as shown in the Eq.(2).

$$I_{ph} = I_{ph_{STC}}\frac{G}{G_{STC}}(1+\alpha_I(T_c - T_{c_{STC}})) \quad (2)$$

where $I_{ph_{STC}}$ is the photo-current in short-circuit at the standard test condition (STC), G is the global radiation that receives the PV cell, G_{STC} is the irradiance at STC ($1000W/m^2$), α_I is the temperature coefficient given by the manufacturer of the PV module ($\%/°C$), T_c temperature of the PV cell (C), $T_{c,STC}$ is the temperature on STC (25°C).
However, these equations do no take into account the shape of the shading neither the optical properties of the shadow present on PV array. The photo-current in Eq.(1) depends on uniform irradiation.

2.2 Proposed Shaded PV-cell model

Fig.1 shows the general schematic of the proposed PV model. The model inputs represent the environmental variables such as solar irradiation, temperature, matrix of shadow and the electrical parameters of PV cells. The model outputs are PV module voltage and PV module current, done variations on the load resistance. The proposed model takes into account the electrical and thermal behaviours of each cell of a PV module. The configuration of a cell interconnection circuit suitable for powering a given application is obtained by calculating the number of cells in series needed to generate a convenient voltage $V_o(t)$, and the number of strings in parallel needed to produce sufficient current $I_o(t)$. Normally, a PV panel is composed on a set of cells (e.g., 36, 60, 72), and a set of bypass-diodes.

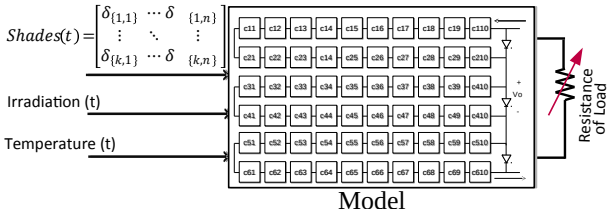

Fig. 1 General schematic of the proposed PV-module model

Direct and indirect radiations on all cells of a panel have not the same impact because of buildings or trees shades, atmosphere fluctuation, existence of clouds and daily sun angle changes. The impact of the non-uniform irradiation on the production of energy depends on several aspects as cell material, magnitude of the area of shade, bypass diode placement [12], string configuration, etc. For this reason, PV module can have different values of I_{ph} for each cell. Under partial shading operation, the unshaded cells of the module receive a solar irradiation at certain level, while the shaded cells lesser irradiation. By definition, the global irradiation is composed of three radiations: the direct radiation (G_D), the diffuse radiation (G_d), and the reflected radiation (G_f) as shown in Eq.(3) .

$$G_T = G_D + G_d + G_r \quad (3)$$

The approximation I_{ph}≈I_{sc} considers standard operating conditions with no shading. However, irradiation current depends linearly on the incident light and the area of shading, as depicted in Fig.2.

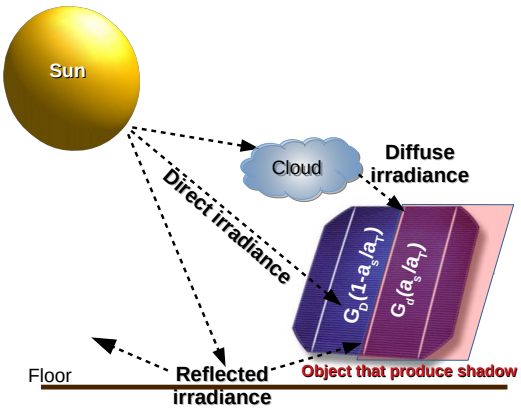

Fig. 2 The irradiance current of a cell as a linear combination of global and diffuse light

Olalla [13] showed the new relation of the photo-current in function of a linear combination of the global and diffuse

irradiation as seen in Eq.(4). Term 1 represents the direct solar radiation with the factor of the unshaded cell. Term 2 represents the non-direct radiation that arrives at the cell with the factor of shaded cell.

$$\begin{aligned} I_{ph} &= \underbrace{(G_D \cdot (1-\frac{a_s}{a_T})}_{1} + \underbrace{((G_d+G_r)\cdot\frac{a_s}{a_T})}_{2} \cdot \frac{I_{phTi}}{G_{STC}} \\ I_{ph} &= \underbrace{\frac{G_D \cdot I_{phTi}}{G_{STC}} \cdot (1-\frac{a_s}{a_T})}_{1} + \underbrace{\frac{(G_d+G_r)\cdot I_{phTi}}{G_{STC}} \cdot \frac{a_s}{a_T}}_{2} \end{aligned} \quad (4)$$

where G_{STC}= 1000 W/m^2, a_T, the total area of the cell, a_s, the shadow area of the cell and I_{phTi} the input current of each cell without shadow. Eq.(5) shows two attenuation factors δ_1 representing the unshaded part and δ_2 the shaded part.

$$\begin{aligned} \delta_1 &= \frac{G_D}{G_{STC}} \cdot (1-\frac{a_s}{a_T}) \\ \delta_2 &= \frac{(G_d+G_r)}{G_{STC}} \cdot \frac{a_s}{a_T} \end{aligned} \quad (5)$$

The effective input current produced by the cell, is showed in Eq.(6) in function of theses factor.

$$\begin{aligned} I_{ph} &= (\delta_1+\delta_2)\cdot I_{phTi} \\ I_{ph} &= \delta \cdot I_{phTi} \end{aligned} \quad (6)$$

δ is the total attenuation factor ($0 \leq \delta \leq 1$). PV cells can have different value of δ and these modifications allow to build a shadow matrix $M\delta(t)$ as shown in Eq. (7).

$$\delta(t) = \begin{bmatrix} \delta_{11} & \delta_{12} & \delta_{13} & \delta_{14} & \delta_{15} & \delta_{16} & \delta_{17} & \delta_{18} & \delta_{19} & \delta_{110} \\ \delta_{21} & \delta_{22} & \delta_{23} & \delta_{24} & \delta_{25} & \delta_{26} & \delta_{27} & \delta_{28} & \delta_{29} & \delta_{210} \\ \delta_{31} & \delta_{32} & \delta_{33} & \delta_{34} & \delta_{35} & \delta_{36} & \delta_{37} & \delta_{38} & \delta_{39} & \delta_{310} \\ \delta_{41} & \delta_{42} & \delta_{43} & \delta_{44} & \delta_{45} & \delta_{46} & \delta_{47} & \delta_{48} & \delta_{49} & \delta_{410} \\ \delta_{51} & \delta_{52} & \delta_{53} & \delta_{54} & \delta_{55} & \delta_{56} & \delta_{57} & \delta_{58} & \delta_{59} & \delta_{510} \\ \delta_{61} & \delta_{62} & \delta_{63} & \delta_{64} & \delta_{65} & \delta_{66} & \delta_{67} & \delta_{68} & \delta_{69} & \delta_{610} \end{bmatrix} \quad (7)$$

The proposed model uses the energy flows that convert sunlight into electrical energy. PV cell modeling can be done with different levels of accuracy, depending of the purposes user. Eq.(1) gives not accurate information about the effects of inherent variations on the cell performance (influenced by the uniformity of cell fabrication processes) and on the array performance. In order to describe each electrical behaviour of each PV cell of a PV module, the photo-current term I_{ph} is replaced by the relation shown in Eq.(6)

$$\begin{aligned} I = \delta I_{phTi} - I_o \left[e^{\frac{V_c+IR_s}{V_t}} - 1 \right] \\ - \frac{V_c+IR_s}{R_{sh}} \left[1 + k \left(1 - \frac{V_c+IRs}{V_{br}} \right)^{-n} \right] \end{aligned} \quad (8)$$

Eq (8) describes the behaviour of the interconnection circuit of each PV cell under abnormal, but common, operating conditions, e.g. partial shadowing of the array by nearby structures at any times of the day. A complete description of the effects of electrical mismatches in real interconnection circuits requires the determination of cell operating currents and voltages. Direct measurements of the operating points of PV cells are not possible because of their encapsulation in the panel.

2.3 Proposed Shaded PV-module model with bypass diode

Under non-uniform conditions, PV module can see its performance decreasing because of hot spotting problem. To protect shaded PV cells from breakdown voltage, PV modules are equipped with bypass diodes. The studied PV module (TE2200) has the followed specifications : 60 cells (6x10), multicrystalline, three bypass diodes. The electrical parameters are I_{SC}=8.6(A), V_{oc}=37.2(V), R_s=0.005(Ω), R_{sh}=35(Ω), V_b=-30(V), n=3.4, k=0.01, $P_{MAX_{STC}}$=245(W), $P_{MIN_{STC}}$=240(W).

In a string of nPV cells in series, the conditions for having bypass diode activation are:

$$V_{G_k} = \begin{cases} V_{diode} & if\ n < \frac{V_{shadowed}-V_{bypass}}{V_{non-shadowed}} + 1 \\ \sum_{i=1}^{n} V_{cell_i} & if\ n \geq \frac{V_{shadowed}-V_{bypass}}{V_{non-shadowed}} + 1 \end{cases} \quad (9)$$

$$I_{G_k} = I_{C_1} = I_{C_2} = I_{C_3} = ... = I_{C_n}$$

V_{G_k} is the string of series cells protected by one bypass diode, $V_{shadowed}$ the voltage for shadowed cell, V_{bypass} the forward voltage when the bypass diode turns ON and $V_{nonshadowed}$ the forward voltage for each illuminated cells.

$$\begin{aligned} V_{module} &= V_{G_1} + V_{G_2} + V_{G_3} + ... + V_{G_k} \\ I_{module} &= I_{G_1} = I_{G_2} = I_{G_3} = ... = I_{G_k} \end{aligned} \quad (10)$$

HBG uses nine basic elements or building blocks which may represent physical subsystems, components or phenomena in every energy domains.

Fig. 3 (a) shows the whole HBG design of a PV module. The input parameters are the PV module temperature, the global irradiation that receives the PV module. The three blocks represent 20 cells in series connected to one bypass diode. The element R corresponds to the bypass diode and C is the parasitic capacitance. MR is a variable resistance that allows to obtain the electric behaviour of the PV module (I-V characteristic) varying the resistance value between $[0,\infty)$. It is possible to obtain positive and negative variations of the resistance for achieve the responses of I= $[0,\infty]$ and V=$[V_{OC}, V_{br}]$ in the complete I-V showing the avalanche effect of the PV cell in reverse bias.

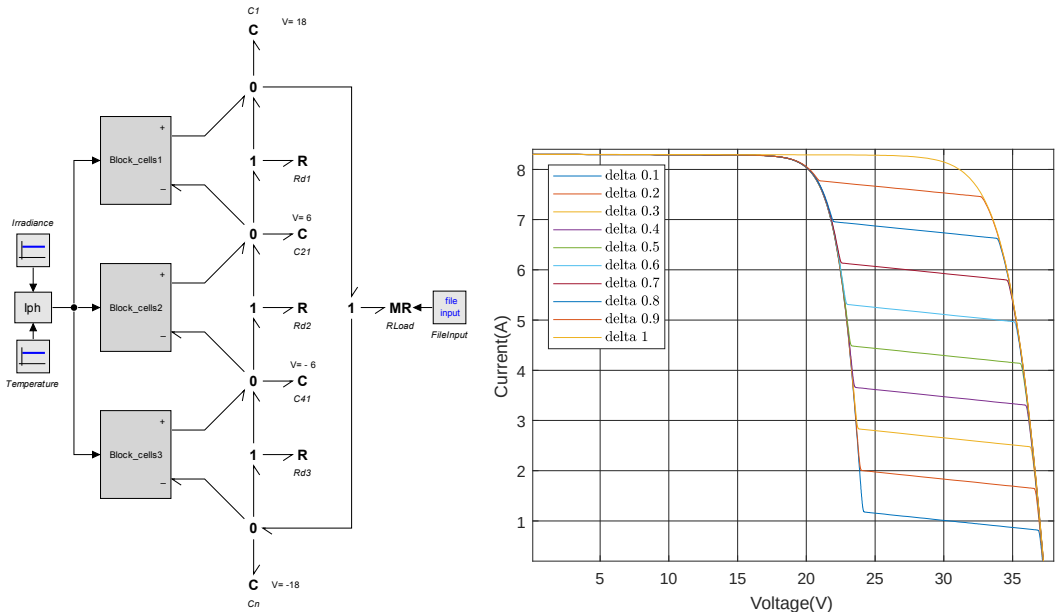

(a) PV module structure with bypass (b) I-V curves for different delta and with diode Bypass

Fig. 3 Shading tests simulation in HBG and I-V curves results

Fig.3 (b) shows the simulation of I-V curves in HBG for different percentage of attenuation factor performed on one group of cells of a PV module. If the string voltage exceeds the transmission voltage of the bypass diode, it becomes active. theoretically, the breakdown voltage is not reached.
The next part explains the different process of image processing of the shadow allowing to characterize complex shading conditions on PV modules.

3 Experimental setup and image processing

The experimental setup was performed in LAAS-CNRS in Toulouse, France (ϕ=43.562093, λ= 1.477460). The I-V characteristics were measured trough a) Curve tracer EKO MP160, b) PV selector EKO 510, c) acquisition software, d) weather station, and e) thermal camera FLIR i-60. Two PV modules (TE2200) were used with one as reference in normal operating and the other to perform shading tests. Fig.4 shows an example of complex shading (a) with the segmentation of PV cells (b) and the segmentation of the shadow area (c). A PV module is composed of 60 cells (6 x 10) with an ideal area of 156 x 156 *mm*. The effective area of the cell is smaller, since the cell is not a square but an octagon. The octagon is divided into four regions representing the cells C5,9; C5,10; C6,9; C6,10. To calculate the attenuation factor δ_2, it is necessary to know the irradiation received by the shaded PV cell. An approximation of the diffuse radiation was performed thanks to a planar Silicon PN photodiode (BPW21R). The BPW21 has a spectral sensitivity of 10 nA/Lx. A digital camera of cellphone Huawei VNS-L31, primary camera 13 MP (f/2.0,1/3",1.12m) with auto-focus was used to capture the image of the PV module with the shadow. The camera was placed on a tripod to record from a fixed position the shadow that affects the panel. The second step consisted in treating the image thanks to the superpixel method allowing to calculate the shading area a_s. The process of estimation of the magnitude of shadow was performed under Matlab2017a. The complete image processing is explained as below:

1. The inclination of the panel is in vertical position.
2. The image is cropped to the width and height of the panel.
3. The presence of shadow is detected using the superpixel algorithm.
4. The image segmentation toolbox is used to isolate the shadow, food fill, and active contours.
5. The toolbox image region analyzer is employed to estimate the magnitude of the shadow area.

Firstly, it is necessary to quantify the complete area of each selected PV cell. The result of the segmentation of the whole panel to determine the area of each selected PV cell is shown in Table 1. Each result value is represented in pixel numbers. The second step consists in isolating and quantifying the shadow area of the selected region on PV module. Table 2 shows the result of the segmentation of the shadow area of each PV cell. Table 3 resumes the results of each affected zone of the shadow to determine the attenuation factor δ. It is calculated knowing the both radiation as mentioned in Eq.(4).

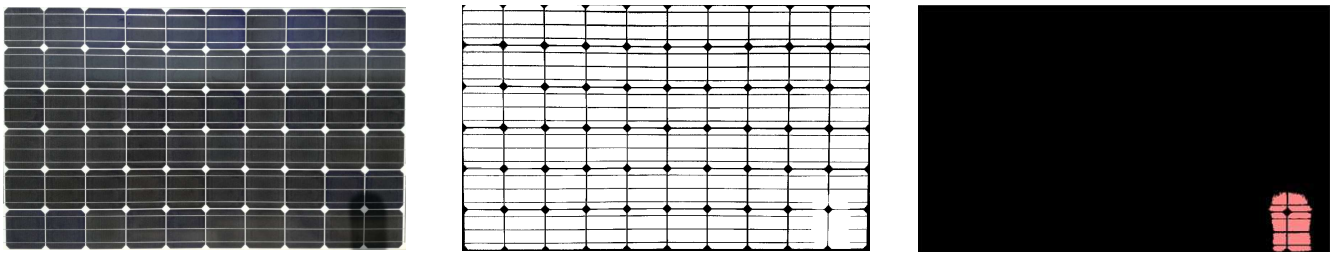

Fig. 4 a) PV module Photography, b) Segmentation of PV cells, c) Segmentation of the shadow area

Cell	Section cell	Area	Subtotal	Total Area
5,9	a	67362	132189	525963
	b	19261		
	c,d	45566		
5,10	a	66607	129406	
	b	44272		
	c,d	18527		
6,9	a	19454	131160	
	b	45944		
	c	45783		
	d	19979		
6,10	a	22183	133208	
	b	45078		
	c	45226		
	d	20721		

Table 1 Quantification of the area of each selected PV Cell

Cell	Section cell	Area	Subtotal	Total Area
5,9	c	8634	22761	164062
	d	14127		
5,10	c	17727	29724	
	d	11997		
6,9	a	7696	37316	
	b	15387		
	c	14233		
	d	6147		
6,10	a	11576	74261	
	b	25462		
	c	25175		
	d	12048		

Table 2 Quantification of the shadow area of each affected PV Cell area

Cell	Cell Area	Shadow Area	a_s (%)	δ (%)
5,9	132189	22761	17.21	82.78
5,10	129406	29724	22.97	77.03
6,9	131160	37316	28.45	71.55
6,10	133208	74261	55.75	44.25

Table 3 Percentage of the shadow area and attenuation factor calculation

4 Experimentation and results

This section presents the results and the validation of the proposed model through two cases. The fist one represents the model without shadow and the second one with a complex shadow on PV module.

4.1 Case 1: Validation of the HBG model in normal operating

For this purpose, measurements of I-V curve of the reference panel is compared with the model. The test is performed the January, 25th, 2018 at 10:40AM with a global irradiation of $624W/m^2$ and a cell temperature of 25°C. In this case $\delta_2 = 0$ since no shadows are visible on PV module. The attenuation factor δ corresponds only to the global radiation that receives PV module. In this case, all the attenuation factor is fixed to 1. Fig.7 shows measurements of I-V curve of the reference panel compared with I-V curve of the model.

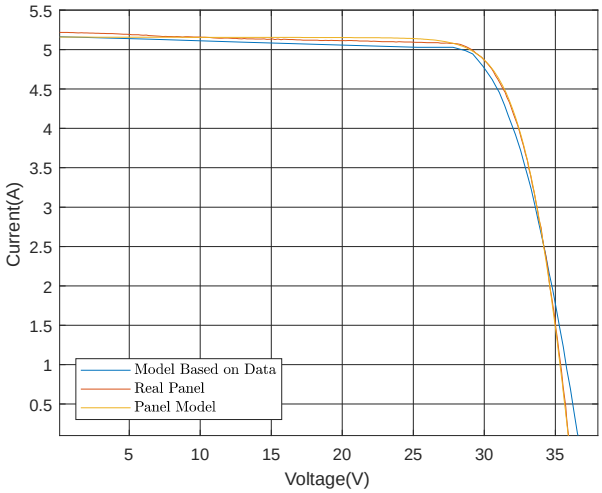

Fig. 5 I-V curves validation in normal operating

The *Mean Square Error* (MSE) result is used to assess modeling accuracy based on the shading ratio. The *MSE* has a good accuracy around of 1.6%. The next case consists in performing an uniform shading case with various shaded PV cell.

4.1.1 Case 2: Validation under complex shading condition

For this purpose, two sheets of paper were placed on the surface of the panel as shown in Fig.6 with a shadow area of $a_s = 0.5$ for the one and $a_s = 0.23$ for the other. The experimentation tests were performed during the February, 9th,

2018 at 12:06PM with a solar irradiation of $387.80 W/m^2$ and a cell temperature of 19°C. Depending on the characteristic of the shadow, the values of the matrix of shadow change during the day inducing some DC power losses.

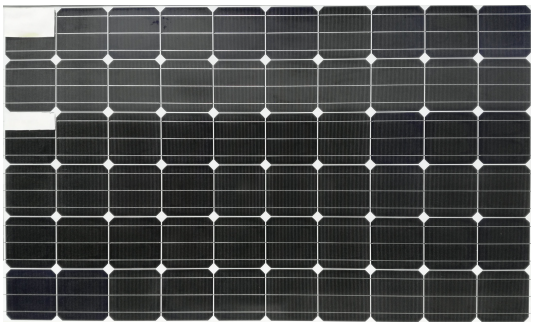

Fig. 6 Shadow test on PV module during the February, 9th, 2018

In function of the shadow position and its area, the attenuation factor δ is calculated and presented in the shadow matrix in Eq. (11). Fig. 7 illustrated the comparison of the model of I-V curves with the experimental I-V in normal operating and in shading conditions. The MSE is 3% for the shading case.

$$\delta(t) = \begin{bmatrix} 0.5 & 1.0 & 1.0 & 1.0 & 1.0 & 1.0 & 1.0 & 1.0 & 1.0 & 1.0 \\ 1.0 & 1.0 & 1.0 & 1.0 & 1.0 & 1.0 & 1.0 & 1.0 & 1.0 & 1.0 \\ 0.77 & 1.0 & 1.0 & 1.0 & 1.0 & 1.0 & 1.0 & 1.0 & 1.0 & 1.0 \\ 1.0 & 1.0 & 1.0 & 1.0 & 1.0 & 1.0 & 1.0 & 1.0 & 1.0 & 1.0 \\ 1.0 & 1.0 & 1.0 & 1.0 & 1.0 & 1.0 & 1.0 & 1.0 & 1.0 & 1.0 \\ 1.0 & 1.0 & 1.0 & 1.0 & 1.0 & 1.0 & 1.0 & 1.0 & 1.0 & 1.0 \end{bmatrix} \quad (11)$$

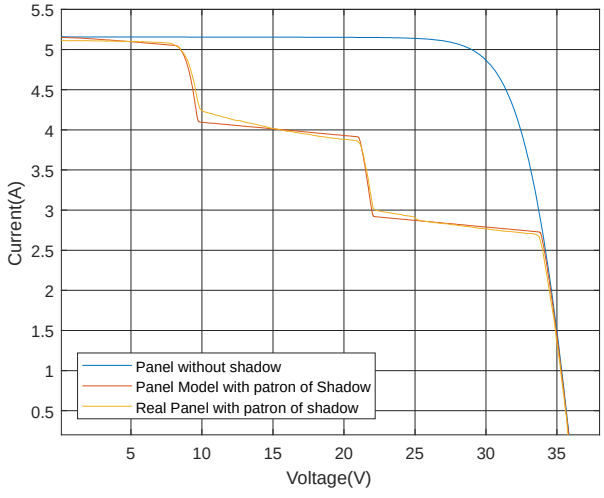

Fig. 7 I-V curves validation under shading conditions

5 Conclusion

The proposed work presented a model able to take into account the effect of complex shading in the I-V curves. The area of shadow was deducted thanks to image processing of PV module using the simple linear iterative clustering (SLIC) algorithm. Moreover the combination of direct and indirect radiation was permitted to obtain the attenuation factor inducing the decrease of the electrical generation under complex shading conditions. The model was validated through experimental tests during various specifics days with an acceptable error.

References

1. M. R. Maghami, H. Hizam, C. Gomes, M. A. Radzi, M. I. Rezadad, and S. Hajighorbani, "Power loss due to soiling on solar panel: A review," *Renewable and Sustainable Energy Reviews*, vol. 59, pp. 1307 – 1316, 2016.
2. Y. E. Basri, M. Bressan, L. Seguier, H. Alawadhi, and C. Alonso, "A proposed graphical electrical signatures supervision method to study pv module failures," *Solar Energy*, vol. 116, pp. 247 – 256, 2015.
3. M. Bressan, Y. E. Basri, A. Galeano, and C. Alonso, "A shadow fault detection method based on the standard error analysis of i-v curves," *Renewable Energy*, vol. 99, pp. 1181 – 1190, 2016.
4. K. A. Kim and P. T. Krein, "Reexamination of photovoltaic hot spotting to show inadequacy of the bypass diode," *IEEE Journal of Photovoltaics*, vol. 5, no. 5, pp. 1435–1441, Sept 2015.
5. N. Mishra, A. S. Yadav, R. Pachauri, Y. K. Chauhan, and V. K. Yadav, "Performance enhancement of pv system using proposed array topologies under various shadow patterns," *Solar Energy*, vol. 157, pp. 641 – 656, 2017.
6. E. I. Batzelis, P. S. Georgilakis, and S. A. Papathanassiou, "Energy models for photovoltaic systems under partial shading conditions: a comprehensive review," *IET Renewable Power Generation*, vol. 9, no. 4, pp. 340–349, 2015.
7. M. Bressan, A. Gutierrez, L. G. Gutierrez, and C. Alonso, "Development of a real-time hot-spot prevention using an emulator of partially shaded pv systems," *Renewable Energy*, vol. 127, pp. 334–343, 2018.
8. A. Mohapatra, B. Nayak, P. Das, and K. B. Mohanty, "A review on mppt techniques of pv system under partial shading condition," *Renewable and Sustainable Energy Reviews*, vol. 80, pp. 854 – 867, 2017.
9. A. Gutiérrez Galeano, M. Bressan, F. Jiménez Vargas, and C. Alonso, "Shading ratio impact on photovoltaic modules and correlation with shading patterns," *Energies*, vol. 11, no. 4, 2018. [Online]. Available: http://www.mdpi.com/1996-1073/11/4/852
10. G. R. Walker, "Evaluating mppt converter topologies using a matlab pv model," *Australian Journal of Electrical & Electronics Engineering*, vol. 21, no. 1, pp. 49–55, 2001. [Online]. Available: https://eprints.qut.edu.au/63580/
11. J. Bishop, "Computer simulation of the effects of electrical mismatches in photovoltaic cell interconnection circuits," *Solar cells*, vol. 25, no. 1, pp. 73–89, 1988.
12. S. Silvestre, A. Boronat, and A. Chouder, "Study of bypass diodes configuration on {PV} modules," *Applied Energy*, vol. 86, no. 9, pp. 1632 – 1640, 2009.
13. C. Olalla, D. Clement, D. Maksimovic, and C. Deline, "A cell-level photovoltaic model for high-granularity simulations," *2013 15th European Conference on Power Electronics and Applications, EPE 2013*, 2013.